HHS Public Access

Author manuscript

J Am Chem Soc. Author manuscript; available in PMC 2021 November 25.

Published in final edited form as:

J Am Chem Soc. 2020 November 25; 142(47): 20058–20065. doi:10.1021/jacs.0c09399.

Crescent-shaped supramolecular tetrapeptide nanostructures

Yin Wang[1,2], **Zhao Li**[1], **Yulia Shmidov**[3], **Ryan J. Carrazzone**[1], **Ronit Bitton**[3], **John B. Matson**[1,*]

[1]Department of Chemistry, Virginia Tech Center for Drug Discovery, and Macromolecules Innovation Institute, Virginia Tech, Blacksburg, VA 24061, United States

[2]School of Pharmacy, Shanghai Jiao Tong University, Shanghai 200240, People's Republic of China

[3]Department of Chemical Engineering and the Ilse Katz Institute for Nanoscale Science and Technology, Ben-Gurion University of the Negev, Beer-Sheva 84105, Israel

Abstract

Self-assembly of amphiphilic peptide-based building blocks gives rise to a plethora of interesting nanostructures such as ribbons, fibers, and tubes. However, it remains a great challenge to employ peptide self-assembly to directly produce nanostructures with lower symmetry than these highly symmetric motifs. We report here our discovery that persistent and regular crescent nanostructures with a diameter of 28±3 nm formed from a series of tetrapeptides with the general structure **Ad$K_S$$K_S$EX** (Ad = adamantyl group, K_S = lysine residue functionalized with an S-aroylthiooxime (SATO) group, E = glutamic acid residue, and X = variable amino acid residue). In the presence of cysteine, the biological signaling gas hydrogen sulfide (H_2S) was released from the SATO units of the crescent nanostructures, termed peptide-H_2S donor conjugates (PHDCs), reducing levels of reactive oxygen species (ROS) in macrophage cells. Additional in vitro studies showed that the crescent nanostructures alleviated cytotoxicity induced by phorbol 12-myristate 13-acetate (PMA) more effectively than common H_2S donors and a PHDC of a similar chemical structure, **Ad$K_S$$K_S$E**, that formed short nanoworms instead of nanocrescents. Cell internalization studies indicated that nanocrescent-forming PHDCs were more effective in reducing ROS levels in macrophages because they entered into and remained in cells better than nanoworms, highlighting how nanostructure morphology can affect bioactivity in drug delivery.

Graphical Abstract

*Corresponding Author: jbmatson@vt.edu.

Author Contributions

The manuscript was written through contributions of all authors.

ASSOCIATED CONTENT

Supporting Information

The Supporting Information is available free of charge on the ACS Publications website.

Detailed experimental section, additional cell studies, and additional characterization (ESI-MS, UV−vis, circular dichroism) (PDF)

The authors declare no competing financial interest.

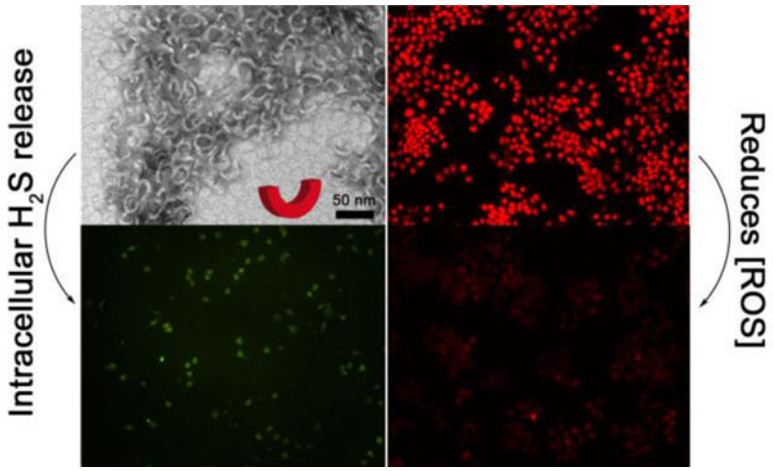

Introduction

Self-assembly of organic compounds can be harnessed to access supramolecular nanostructures with a wide range of shapes, including spheres,[1–2] toroids,[3–4] cylinders,[5–6] helices,[7–8] sheets,[9–10] and others, with many resembling well-known biological nanostructures such as vesicles,[11] microtubules,[12] and the DNA double helix.[13] Although not as familiar as these highly symmetric examples, a range of biological nanostructures with fewer symmetry elements also exist. Examples include the truncated cone-shaped envelope of the HIV virus,[14] the wedge-and-stem shape of nucleosomes,[15–16] and the crescent-shaped lipoprotein membranes that form poxviruses.[17] In all cases, the asymmetric shape serves the biological function of the nanostructure. For instance, crescent-shaped membranes in the vaccinia virus are vital for the formation of mature virions.[18] Similar to natural nanostructures, synthetic nanostructures with relatively few symmetry elements made by self-assembly are also rare, and as in biological examples, their unique shapes may enable functions that highly symmetric nanostructures cannot.

Among the classes of synthetic small molecules capable of self-assembly into nanostructures, peptides are perhaps the most widely studied due to their biodegradability, high degree of tunability, and capacity for several types of non-covalent interactions.[5–6, 19–21] Beyond this, they can be quickly synthesized and purified with direct sequence control. Our group is interested in the aqueous self-assembly of short peptides and peptide derivatives into unusual nanostructures and their applications in biology and other areas.[22–27] Here we report on our recent discovery of an aromatic peptide amphiphile that self-assembles into crescent-shaped nanostructures. Crescent-shaped inorganic nanostructures have been prepared through various means, and their crescent shape affords unique properties.[28–33] In contrast, it remains a great challenge to produce crescent nanostructures from peptides, or any small organic molecule, through a direct self-assembly approach. In fact, we are aware of only one such example from Xu and coworkers,[34] who found that a cationic phosphotetrapeptide containing three D-amino acid residues formed crescent nanostructures upon removal of the phosphate group by alkaline phosphatase. These peptide assemblies showed remarkable bioactivity, accumulating on the endoplasmic reticulum to

induce death in cancer cells, where the crescent shape was critical for membrane disruption. This discovery highlights the need to further study how crescent nanostructures can be synthesized and applied in biology and medicine.

Intrigued by the ability of crescent-shaped nanostructures to induce unexpected biological activity in natural and synthetic systems, we investigated here how crescent-shaped peptide assemblies could influence the delivery and bioactivity of the biological signaling gas hydrogen sulfide (H_2S). H_2S was long thought to be only a poisonous gas, but its biological signaling roles were discovered in 1996.[35] Since then, a wide variety of studies have shown that H_2S mediates numerous (patho)physiological processes, including vasorelaxation, oxidative stress reduction, and inflammation.[36–39] However, these results were mainly acquired by using inorganic sulfide salts such as sodium sulfide (Na_2S) or sodium hydrosulfide (NaSH) as H_2S sources.[40–41] Recognizing that these sulfide salts were not ideal compounds for studying H_2S biology, researchers have developed several classes of stimuli-responsive, H_2S-releasing compounds (termed H_2S donors) over the past several years.[42–44] H_2S donors with targeting capabilities and varying release rates have shown that the method of delivery can greatly influence the bioactivity of this gas.[23–24] However, despite this progress, most H_2S donors lack good water solubility and have limited means for cell internalization, hindering H_2S-based treatments due to the reactive and transient nature of this signaling molecule. Based on our discovery of a short peptide capable of releasing H_2S that self-assembles into crescent nanostructures (Figures 1A and 1B), we asked how the crescent shape would influence the bioactivity of this uniquely shaped H_2S donor. Specifically, based on the cell internalizing properties of natural and synthetic crescent-shaped nanostructures noted above, we hypothesized that crescent-shaped H_2S-releasing nanostructures would be more effective at reducing oxidative stress in macrophages, a known property of H_2S,[36, 45–46] than small molecule H_2S donors or peptide-based H_2S donors that take on other shapes.

Results and Discussion

We report here on a class of amphiphilic peptide-H_2S donor conjugates (PHDCs) that unexpectedly self-assembled into discrete, crescent-shaped nanostructures in aqueous solution. To make the PHDCs, we prepared a peptide of the structure **Ad$K_S$$K_S$EE** (Ad = adamantyl group, K_S = lysine residue functionalized with an H_2S-releasing *S*-aroylthiooxime (SATO) group, E = glutamic acid residue; Figure 1A). We originally developed the SATO group due to its ability to generate H_2S in response to thiols,[47] but we found that its inclusion in peptides generates a variety of self-assembled morphologies; for example, PHDCs containing two K_S and two E residues form persistent nanohelices or nanoribbons of various sizes depending on the specific sequence.[23–25] Here we included for the first time the bulky Ad group with the idea that it would provide additional hydrophobic interactions beyond those of the SATO groups, while also contributing steric hindrance during the self-assembly process. Detailed synthetic procedures and characterization can be found in the Supporting Information (Figures S1 and S2).

PHDC **Ad$K_S$$K_S$EE** spontaneously self-assembled upon dissolution in 10 mM phosphate buffer (pH 7.4) at room temperature. The aggregation of PHDC **Ad$K_S$$K_S$EE** in aqueous

solution was first confirmed by the Nile Red assay, where the fluorescence intensity increased as the concentration of PHDC increased (Figure S3), indicating solubilization of Nile Red in the hydrophobic domain.[48] The critical aggregation concentration (CAC) was calculated to be 27 μM, similar to our previous CAC measurements on related PHDCs.[23–24] Next, we examined the morphology of the assemblies by both conventional and cryogenic transmission electron microscopy (TEM). Both techniques revealed that PHDC **Ad$K_S$$K_S$EE** assembled into crescent nanostructures in aqueous solution (Figures 1C and 1D) with average external diameters of 28±3 nm and average widths of 5±1 nm. The aggregation number was further characterized by static light scattering (SLS), showing that on average 600 **Ad$K_S$$K_S$EE** molecules assemble to form each crescent nanostructure. This value was close to our estimate of 560 based on the volume of an average nanocrescent, calculated using its dimensions from TEM, and the estimated volume of an **Ad$K_S$$K_S$EE** molecule (see Supporting Information).

We also ran experiments to probe the secondary structure and the reactivity of these assemblies. Circular dichroism (CD) spectroscopy showed a strong negative absorption at 320 nm (Figure 1E), a peak consistent with an absorption peak of the SATO unit and also observed in the UV-vis spectrum (Figure S4), indicating that SATOs were arranged in a highly ordered fashion within the nanostructures. Additional SATO absorptions in the peptide region (190–240 nm) make it difficult to draw firm conclusions from the CD spectrum on peptide secondary structure, but some contributions from β-sheet structures are likely due to the extended nature of these nanostructures.[49] Therefore, we used the common Thioflavin-T (ThT) assay to evaluate whether β-sheets were present in the nanostructures.[50] We found that ThT fluorescence intensity increased dramatically when the **Ad$K_S$$K_S$EE** crescents were treated with ThT solution, indicating that β-sheets exist within the crescent nanostructures (Figure S5A). Finally, consistent with other SATO-based H_2S donors,[23, 26–27, 51] **Ad$K_S$$K_S$EE** released H_2S in the presence of cysteine (Cys) over 3 h, with a peaking time of 125 ±15 min (black curve, Figure 1F), while minimal H_2S was detected from experiments without Cys (blue curve, Figure 1F).

To gain more insight into the molecular requirements for crescent nanostructure formation, we synthesized several control molecules. As shown in Figures S6A and B, replacing the Ad unit with other capping agents at the N terminus (acetyl or cyclohexyl) generated twisted nanoribbons. Given that the only difference among these three molecules is the capping agent, we speculate that the bulky Ad unit in crescent-forming PHDC **Ad$K_S$$K_S$EE** hinders the formation of long-range β-sheets during self-assembly, consistent with short nanostructures observed in other SATO-containing peptides with a bulky C-terminus.[24] In sharp contrast, acetyl or cyclohexyl groups are smaller and more planar, allowing for closer packing; therefore, long-range β-sheets can form during self-assembly into long nanoribbons (Figure S5). Replacing one of the K_S residues with a phenylalanine residue also resulted in the disappearance of the crescent morphology (Figure S6C). Finally, changing both K_S residues to K_O residues (where K_O represents a non-H_2S-releasing benzyl oxime-functionalized lysine residue) or K_{FBA} residues (where K_{FBA} represents a 4-formylbenzoic acid-functionalized lysine residue), also afforded irregular aggregates (Figures S7–S8),

indicating that the N-terminal Ad group and the K_S residues, at least in these PHDCs, are important for nanocrescent formation.

In contrast, we found that the crescent morphology was largely insensitive to the choice of amino acid residue on the C terminus. As shown in Figure 2, replacing the C-terminal E residue in the original design with a cationic histidine (H) residue (Figures 2A and 2E), a nonionic serine (S) residue (Figures 2B and 2F), or an anionic aspartic acid (D) residue (Figures 2C and 2G) did not change the morphology, implying that **AdKsKsEX** (X = variable residue) is a consensus sequence for forming self-assembled nanocrescents. This was also confirmed by the similar CD spectra for these three control peptides (Figure S10). More importantly, these results also demonstrated that this peptide design is robust enough to enable the incorporation of various functional units at the C terminus without altering the supramolecular architecture, which is a challenging topic in supramolecular assembly.[52]

Finally, we also tested the main tripeptide segment, **AdKsKsE**, for the formation of nanocrescents. In this case we installed a C-terminal carboxylic acid instead of the carboxamide used in **AdKsKsEE**, thus maintaining the two carboxylate units in the original peptide design (Figure 2D). Surprisingly, despite its similarity in structure and charge to the original nanocrescent-forming PHDC **AdKsKsEE**, it assembled into short nanoworms with average lengths of 33±2 nm (Figure 2H). This result indicated that the C-terminal amino acid residue is necessary for the formation of nanocrescents. Thus, **AdKsKsE** provided an ideal control peptide for assessing our hypothesis regarding nanostructure shape and cell internalization because it has a similar chemical structure and an identical charge to **AdKsKsEE**, but it forms short nanoworms rather than nanocrescents. Also, both **AdKsKsE** and **AdKsKsEE** release similar amounts of H_2S because they both contain two SATO units, although release is somewhat faster from **AdKsKsE** (Figure S13).

Given that H_2S can reduce inflammation and related oxidative stress,[36, 53] we then asked whether H_2S release from **Ad$K_S$$K_S$EE** or **Ad$K_S$$K_S$E** could decrease intracellular ROS production. We tested these two peptides specifically, along with relevant controls, because this pair provided a method to assess how the crescent shape would affect bioactivity. In other words, we asked whether persistent crescent-shaped nanostructures would be more effective than flexible worms of a similar size at delivering H_2S to protect cells from ROS-induced damage. In these experiments, RAW 264.7 macrophage cells were chosen as a model because they generate a considerable amount of ROS when incubated with phorbol 12-myristate 13-acetate (PMA).[54–55] Dihydroethidium (DHE) was employed as an ROS sensing fluorescent probe.[56]

As shown in the first row of Figure 3, the control group (RAW 264.7 cells without any treatment) exhibited a dimly red fluorescent signal, indicating that a small amount of ROS was naturally generated within these cells as a product of normal metabolism of oxygen, consistent with previous reports.[57] However, after treatment with PMA, the red fluorescent signal from DHE became much brighter, implying that ROS had accumulated in cells (Figure 3, second row). Addition of Cys or the combination of Cys and non-H_2S-releasing control peptide **Ad$K_O$$K_O$EE** to PMA-treated cells generated a weaker red fluorescent signal compared with the PMA group (Figure 3, third and fourth rows). However, in both cases the

intensity was still much higher than that of the untreated cells, implying that Cys cannot completely inhibit PMA-induced overproduction of ROS. In contrast, co-incubation of **AdK$_S$K$_S$E** and Cys with PMA-treated cells led to a lower red fluorescent signal, indicating that H_2S released from nanoworm-forming **AdK$_S$K$_S$E**, could suppress the production of ROS (Figure 3, fifth row). These results are consistent with previous studies using NaHS, showing that H_2S reduces ROS production in macrophages.[58–59]An improved effect was found in cells treated with both nanocrescent-forming **AdK$_S$K$_S$EE** and Cys (Figure 3, sixth row), with a fluorescence intensity that was the lowest among all the treatment groups and comparable to that of the control group that lacked PMA.

Convinced that **AdK$_S$K$_S$EE** could quench ROS in the presence of Cys (Figure 3), we next explored its anti-inflammatory activity on RAW 264.7 cells. H_2S can alleviate inflammation caused by ROS, but this protective capacity has not been tested widely on sustained H_2S donors.[60–61] More importantly, slow-releasing H_2S donors frequently lead to enhanced biological effects compared to instantaneously released Na_2S.[62–63] Thus, we envisioned that H_2S released from **AdK$_S$K$_S$EE** might rescue RAW 264.7 cells from induced oxidative stress. First, we demonstrated that **AdK$_S$K$_S$EE** was nontoxic to RAW 264.7 cells at concentrations up to 200 μM (Figure S14). In contrast, PMA induced significant cytotoxicity at concentrations as low as 1 μg/mL (Figure 4A).

In treatment studies, RAW264.7 cells were pretreated with PMA for 1 h, a period consistent with previous reports,[54] then **AdK$_S$K$_S$EE** and Cys were added without removing PMA solution. Cells were subsequently cultured for another 3 h before analyzing viability. Compared to the PMA-only treatment group, cell viability increased dramatically when cells were co-treated with PMA and **AdK$_S$K$_S$EE**+Cys (Figure 4A). For example, exposure of PMA to cells at 2 μg/mL decreased cell viability to 67% while viability increased to 95% by co-treatment with **AdK$_S$K$_S$EE**+Cys. Similar increases in viability were observed in treatments with higher or lower levels of PMA.

To further demonstrate that sustained H_2S release was responsible for imparting protection to macrophages in the presence of PMA, several control studies were carried out (Figure 4B). Neither treatment with Cys alone nor treatment with a combination of the non-H_2S-releasing control peptide (**AdK$_O$K$_O$EE**) and Cys showed any protective effect. We also compared **AdK$_S$K$_S$EE** to two traditional H_2S donors under the same experimental conditions, sodium sulfide (Na_2S), a fast-releasing H_2S donor, and GYY4137, a slow-releasing H_2S donor.[64] Neither affected cell viability. PHDC **AdK$_S$K$_S$E**, which slowly releases H_2S but does not form crescents, exhibited some cell protective ability, but it was not as good as **AdK$_S$K$_S$EE**, consistent with results shown in Figure 3. Taken together, these experiments suggest that **AdK$_S$K$_S$EE** could be used as a powerful H_2S delivery platform.

Given the identical conditions and equimolar amounts of **AdK$_S$K$_S$E** and **AdK$_S$K$_S$EE** used in these experiments, the difference in ability to reduce ROS production and protect cells likely stems from the different self-assembled morphologies of these two PHDCs. We hypothesized that nanocrescent-forming **AdK$_S$K$_S$EE** enters and remains in cells to a greater extent than nanoworm-forming **AdK$_S$K$_S$E** due to its unusual morphology. We initially based this hypothesis on Xu's work on positively charged crescent nanostructures,[34] but the

negatively charged nanostructures used in this work would not be expected to bind cell membranes as strongly. We also recognized that the difference in H_2S release rates (**AdK$_S$K$_S$EE** releases H_2S more slowly than **AdK$_S$K$_S$E**) could be responsible for the greater protection observed from **AdK$_S$K$_S$EE**. To test our hypothesis, we conducted cell uptake experiments on PHDCs **AdK$_S$K$_S$EE** and **AdK$_S$K$_S$E**. Because the peptides themselves did not have sufficient fluorescence brightness for imaging, and addition of a fluorophore to their structure would likely change their morphology, we evaluated cell uptake by measuring the amount of H_2S produced inside the cells using an H_2S-selective fluorescent probe, WSP-5.[65]

In these cell uptake experiments, we aimed to quantify cumulative H_2S release over 3 h, corresponding to cumulative intracellular PHDC accumulation over this time period. The period of 3 h was chosen to be consistent with the treatment time used in cell viability assays (Figure 4) and because H_2S release would be complete or nearly complete from both nanostructures over this period. In the first step, macrophage cells were pre-treated with WSP-5 for 30 min, allowing the cells to internalize this pro-fluorophore (Figure 5A). After washing to remove excess WSP-5, PHDCs **AdK$_S$K$_S$EE** and **AdK$_S$K$_S$E** were added, allowing 3 h for uptake of the nanostructures. The cells were then washed to remove any PHDC that was not internalized. Next, Cys was added to induce H_2S release from the internalized nanostructures, generating a fluorescent output from WSP-5 corresponding to the amount of PHDC internalized over the 3 h incubation time. Any H_2S release triggered by endogenous thiols prior to addition of Cys would also have been captured by WSP-5, minimizing the effects of different H_2S release behaviors from the **AdK$_S$K$_S$EE** and **AdK$_S$K$_S$E** nanostructures on the fluorescence intensity. A treatment group with no PHDC (Cys only) was also included as a negative control.

The results of this experiment showed that a small amount of fluorescence was observed in the Cys-only control group, as expected, corresponding to endogenous H_2S captured by WSP-5 (Figure 5, row 1). In contrast, the green fluorescence within the cells was much brighter in the PHDC treatment groups, and cells treated with **AdK$_S$K$_S$EE** (Figure 5, row 3) were 2-fold brighter than cells treated with **AdK$_S$K$_S$E** (Figure 5, row 2). Thus, nanocrescent-forming **AdK$_S$K$_S$EE**, which releases H_2S more slowly than nanoworm-forming **AdK$_S$K$_S$E**, generated more intracellular H_2S. These results indicate that more **AdK$_S$K$_S$EE** than **AdK$_S$K$_S$E** entered into macrophages and released H_2S over the entire course of this experiment. We also conducted a similar experiment designed to measure instantaneous intracellular PHDC concentration after 3 h, in contrast to cumulative intracellular PHDC concentration as shown in Figure 5. The results were similar, with twice as much H_2S, a proxy for PHDC, detected for **AdK$_S$K$_S$EE** versus **AdK$_S$K$_S$E** (Figure S15). Although these results do not directly confirm differences in cell uptake between the two types of nanostructures, our use of H_2S release as a proxy for cell uptake supports our hypothesis that the **AdK$_S$K$_S$EE** nanocrescents more effectively reduce ROS levels in macrophages than the **AdK$_S$K$_S$E** nanoworms because they are internalized and retained better inside the cells.

Conclusions

In summary, we have reported a strategy to prepare crescent nanostructures from a series of adamantane-functionalized tetrapeptides with the general structure **Ad$K_S$$K_S$EX**. Our results showed that these crescent nanostructures only formed when an N-terminal adamantyl group was included in the structure, but they tolerated changes in the C-terminal amino acid. Focusing on PHDC **Ad$K_S$$K_S$EE**, we found that these crescent nanostructures released H_2S steadily over the course of 3 h when triggered with Cys. *In vitro* cell studies further demonstrated that the released H_2S could reduce ROS levels and mitigate toxicity induced by PMA in RAW 264.7 macrophage cells better than common H_2S donors. Additionally, nanocrescent-forming PHDC **Ad$K_S$$K_S$EE** was more effective than a control nanoworm-forming PHDC with a similar structure (**Ad$K_S$$K_S$E**), which we attributed to the ability of the nanocrescents to enter and remain in cells better than the nanoworms.

These results highlight how subtle variation in amphiphilic peptide design can regulate the resulting self-assembled morphology, thereby affecting the H_2S release behavior, and further influencing the resultant bioactivity. Because various amino acid residues could be installed on the PHDC C-terminus while maintaining the nanocrescent morphology, we anticipate that this strategy could serve as a general method to construct crescent nanostructures with different functional groups. Furthermore, this peptide design is a new addition to the aromatic peptide amphiphile family, and the general design driving nanocrescent formation discovered here may find other applications in the biomedical field. Finally, this work also shows how synthetic nanostructures with less symmetry than spheres, rods, and other highly symmetric structures may have enhanced properties in biological applications, reminiscent of natural nanostructures with unusual shapes that afford specialized functions.

Supplementary Material

Refer to Web version on PubMed Central for supplementary material.

ACKNOWLEDGMENT

This work was supported by the National Science Foundation (DMR-1454754) and the National Institutes of Health (R01GM123508). We also acknowledge the Dreyfus foundation for supporting these studies through a Camille Dreyfus Teacher-Scholar Award to J.B.M. We acknowledge Prof. Padmavathy Rajagopalan (Virginia Tech) for sharing RAW 264.7 macrophage cells, Prof. Mark Van Dyke (Virginia Tech) for instrumental assistance, Prof. Sanket A. Deshmukh and Soumil Y. Joshi for assistance with molecular volume estimations, and Kearsley M. Dillon and Samantha J. Scannelli for careful readings of the manuscript. The authors also acknowledge use of facilities within the Nanoscale Characterization and Fabrication Laboratory at Virginia Tech.

REFERENCES

1. Mai YY; Eisenberg A Self-assembly of block copolymers. Chem. Soc. Rev 2012, 41, 5969–5985. [PubMed: 22776960]
2. Kataoka K; Harada A; Nagasaki Y Block copolymer micelles for drug delivery: Design, characterization and biological significance. Adv. Drug Deliv. Rev 2012, 64, 37–48.
3. Hingorani MM; O'Donnell M A tale of toroids in DNA metabolism. Nat. Rev. Mol. Cell Biol 2000, 1, 22–30. [PubMed: 11413486]
4. Kim Y; Li W; Shin S; Lee M Development of toroidal nanostructures by self-assembly: Rational designs and applications. Accounts Chem. Res 2013, 46, 2888–2897.

5. Aida T; Meijer EW; Stupp SI Functional supramolecular polymers. Science 2012, 335, 813–817. [PubMed: 22344437]
6. Cui HG; Webber MJ; Stupp SI Self-assembly of peptide amphiphiles: From molecules to nanostructures to biomaterials. Biopolymers 2010, 94, 1–18. [PubMed: 20091874]
7. Yashima E; Ousaka N; Taura D; Shimomura K; Ikai T; Maeda K Supramolecular helical systems: helical assemblies of small molecules, foldamers, and polymers with chiral amplification and their functions. Chem. Rev 2016, 116, 13752–13990. [PubMed: 27754649]
8. Yang Y; Zhang YJ; Wei ZX Supramolecular helices: Chirality transfer from conjugated molecules to structures. Adv. Mater 2013, 25, 6039–6049. [PubMed: 23966134]
9. Zhuang XD; Mai YY; Wu DQ; Zhang F; Feng XL Two-dimensional soft nanomaterials: A fascinating world of materials. Adv. Mater 2015, 27, 403–427. [PubMed: 25155302]
10. Li C; Li Q; Kaneti YV; Hou D; Yamauchi Y; Mai Y Self-assembly of block copolymers towards mesoporous materials for energy storage and conversion systems. Chem. Soc. Rev 2020, 49, 4681–4736.
11. Walsby AE Gas vesicles. Microbiol. Mol. Biol. Rev 1994, 58, 94–144.
12. Ledbetter MC; Porter KR A microtubule in plant cell fine structure. J. Cell Biol 1963, 19, 239–250. [PubMed: 19866635]
13. Watson JD; Crick FHC Molecular structure of nucleic acids - a structure for deoxyribose nucleic acid. Nature 1953, 171, 737–738. [PubMed: 13054692]
14. Shehu-Xhilaga M; Kraeusslich HG; Pettit S; Swanstrom R; Lee JY; Marshall JA; Crowe SM; Mak J Proteolytic processing of the P2/nucleocapsid cleavage site is critical for human immunodeficiency virus type 1 RNA dimer maturation. J. Virol 2001, 75, 9156–9164. [PubMed: 11533179]
15. McGinty RK; Tan S Nucleosome structure and function. Chem. Rev 2015, 115, 2255–2273. [PubMed: 25495456]
16. Depken M; Schiessel H Nucleosome shape dictates chromatin fiber structure. Biophys. J 2009, 96, 777–784. [PubMed: 19186120]
17. Maruri-Avidal L; Domi A; Weisberg AS; Moss B Participation of vaccinia virus L2 protein in the formation of crescent membranes and immature virions. J. Virol 2011, 85, 2504–2511. [PubMed: 21228235]
18. Liu L; Cooper T; Howley PM; Hayball JD From crescent to mature virion: vaccinia virus assembly and maturation. Viruses-Basel 2014, 6, 3787–3808.
19. Matson JB; Stupp SI Self-assembling peptide scaffolds for regenerative medicine. Chem. Comm 2012, 48, 26–33. [PubMed: 22080255]
20. Worthington P; Langhans S; Pochan D Beta-hairpin peptide hydrogels for package delivery. Adv. Drug Deliv. Rev 2017, 110, 127–136. [PubMed: 28257999]
21. Wang Y; Cheetham AG; Angacian G; Su H; Xie LS; Cui HG Peptide-drug conjugates as effective prodrug strategies for targeted delivery. Adv. Drug Delivery Rev 2017, 110, 112–126.
22. Carter JM; Qian Y; Foster JC; Matson JB Peptide-based hydrogen sulphide-releasing gels. Chem. Commun 2015, 51, 13131–13134.
23. Wang Y; Kaur K; Scannelli SJ; Bitton R; Matson JB Self-assembled nanostructures regulate H_2S release from constitutionally isomeric peptides. J. Am. Chem. Soc 2018, 140, 14945–14951. [PubMed: 30369241]
24. Wang Y; Matson JB Supramolecular nanostructures with tunable donor loading for controlled H_2S release. ACS Appl. Bio Mater 2019, 2, 5093–5098.
25. Wang Y; Yang XZ; Liu TY; Li Z; Leskauskas D; Liu GL; Matson JB Molecular-level control over plasmonic properties in silver nanoparticle/self-assembling peptide hybrids. J. Am. Chem. Soc 2020, 142, 9158–9162.
26. Kaur K; Wang Y; Matson JB Linker-regulated H_2S release from aromatic peptide amphiphile hydrogels. Biomacromolecules 2020, 21, 1171–1178.
27. Qian Y; Kaur K; Foster JC; Matson JB Supramolecular tuning of H2S release from aromatic peptide amphiphile gels: Effect of core unit substituents. Biomacromolecules 2019, 20, 1077–1086. [PubMed: 30676716]

28. Wu LY; Ross BM; Lee LP Optical properties of the crescent-shaped nanohole antenna. Nano Lett 2009, 9, 1956–1961. [PubMed: 19354226]
29. Zhang YH; Liu J; Liu T; You LP; Li XG Supersaturation-controlled synthesis of two types of single-sided ZnO comb-like nanostructures by thermal evaporation at low temperature. J. Cryst. Growth 2005, 285, 541–548.
30. Luo Y; Lei DY; Maier SA; Pendry JB Broadband light harvesting nanostructures robust to edge bluntness. Phys. Rev. Lett 2012, 108, 023901. [PubMed: 22324685]
31. Lu Y; Liu GL; Kim J; Mejia YX; Lee LP Nanophotonic crescent moon structures with sharp edge for ultrasensitive biomolecular detection by local electromagnetic field enhancement effect. Nano Lett 2005, 5, 119–124. [PubMed: 15792424]
32. Goerlitzer ESA; Speichermann LE; Mirza TA; Mohammadi R; Vogel N Addressing the plasmonic hotspot region by site-specific functionalization of nanostructures. Nanoscale Adv 2020, 2, 394–400.
33. Rochholz H; Bocchio N; Kreiter M Tuning resonances on crescent-shaped noble-metal nanoparticles. New J. Phys 2007, 9, 53–53.
34. Feng ZQQ; Wang HM; Wang SY; Zhang Q; Zhang XX; Rodal AA; Xu B Enzymatic assemblies disrupt the membrane and target endoplasmic reticulum for selective cancer cell death. J. Am. Chem. Soc 2018, 140, 9566–9573. [PubMed: 29995402]
35. Abe K; Kimura H The possible role of hydrogen sulfide as an endogenous neuromodulator. J. Neurosci 1996, 16, 1066–1071. [PubMed: 8558235]
36. Wang R Physiological implications of hydrogen sulfide: A whiff exploration that blossomed. Physiol. Rev 2012, 92, 791–896. [PubMed: 22535897]
37. Szabo C Gasotransmitters in cancer: from pathophysiology to experimental therapy. Nat. Rev. Drug Discovery 2016, 15, 185–203. [PubMed: 26678620]
38. King AL; Polhemus DJ; Bhushan S; Otsuka H; Kondo K; Nicholson CK; Bradley JM; Islam KN; Calvert JW; Tao YX; Dugas TR; Kelley EE; Elrod JW; Huang PL; Wang R; Lefer DJ Hydrogen sulfide cytoprotective signaling is endothelial nitric oxide synthase-nitric oxide dependent. Proc. Natl. Acad. Sci. U. S. A 2014, 111, 3182–3187. [PubMed: 24516168]
39. Kimura H Production and physiological effects of hydrogen sulfide. Antioxid. Redox Signaling 2014, 20, 783–793.
40. Zhao WM; Zhang J; Lu YJ; Wang R The vasorelaxant effect of H_2S as a novel endogenous gaseous K-ATP channel opener. Embo J 2001, 20, 6008–6016. [PubMed: 11689441]
41. Jha S; Calvert JW; Duranski MR; Ramachandran A; Lefer DJ Hydrogen sulfide attenuates hepatic ischemia-reperfusion injury: role of antioxidant and antiapoptotic signaling. Am. J. Physiol.-Heart Circul. Physiol 2008, 295, H801–H806.
42. Hartle MD; Pluth MD A practical guide to working with H_2S at the interface of chemistry and biology. Chem. Soc. Rev 2016, 45, 6108–6117. [PubMed: 27167579]
43. Powell CR; Dillon KM; Matson JB A review of hydrogen sulfide (H_2S) donors: Chemistry and potential therapeutic applications. Biochem. Pharmacol 2018, 149, 110–123. [PubMed: 29175421]
44. Zhao Y; Biggs TD; Xian M Hydrogen sulfide (H_2S) releasing agents: chemistry and biological applications. Chem. Commun 2014, 50, 11788–11805.
45. Zhao Y; Pluth MD Hydrogen sulfide donors activated by reactive oxygen species. Angew. Chem. Int. Ed 2016, 55, 14638–14642.
46. Huang CWH; Feng W; Peh MT; Peh K; Dymock BW; Moore PK A novel slow-releasing hydrogen sulfide donor, FW1256, exerts anti-inflammatory effects in mouse macrophages and in vivo. Pharmacol. Res 2016, 113, 533–546. [PubMed: 27687956]
47. Foster JC; Powell CR; Radzinski SC; Matson JB *S*-aroylthiooximes: A facile route to hydrogen sulfide releasing compounds with structure-dependent release kinetics. Org. Lett 2014, 16, 1558–1561. [PubMed: 24575729]
48. Lin YY; Thomas MR; Gelmi A; Leonardo V; Pashuck ET; Maynard SA; Wang Y; Stevens MM Self-assembled 2D free-standing Janus nanosheets with single-layer thickness. J. Am. Chem. Soc 2017, 139, 13592–13595. [PubMed: 28902999]
49. Palmer LC; Stupp SI Molecular self-assembly into one-dimensional nanostructures. Acc. Chem. Res 2008, 41, 1674–1684. [PubMed: 18754628]

50. Khurana R; Coleman C; Ionescu-Zanetti C; Carter SA; Krishna V; Grover RK; Roy R; Singh S Mechanism of thioflavin T binding to amyloid fibrils. J. Struct. Biol 2005, 151, 229–238. [PubMed: 16125973]
51. Qian Y; Altamimi A; Yates SA; Sarkar S; Cochran M; Zhou MJ; Levi-Polyachenko N; Matson JB H_2S-releasing amphiphilic dipeptide hydrogels are potent S. aureus biofilm disruptors. Biomater. Sci 2020, 8, 2564–2576.
52. Su H; Wang FH; Wang YZ; Cheetham AG; Cui HG Macrocyclization of a class of camptothecin analogues into tubular supramolecular polymers. J. Am. Chem. Soc 2019, 141, 17107–17111. [PubMed: 31614088]
53. Gemici B; Wallace JL Anti-inflammatory and cytoprotective properties of hydrogen sulfide. Methods Enzymol 2015, 555, 169–193. [PubMed: 25747480]
54. Hu YM; Li XY; Fang Y; Shi W; Li XH; Chen W; Xian M; Ma HM Reactive oxygen species-triggered off-on fluorescence donor for imaging hydrogen sulfide delivery in living cells. Chem. Sci 2019, 10, 7690–7694. [PubMed: 31803407]
55. Xu J; Zhang Y; Yu H; Gao XD; Shao SJ Mitochondria-targeted fluorescent probe for imaging hydrogen peroxide in living cells. Anal. Chem 2016, 88, 1455–1461. [PubMed: 26695451]
56. Robinson KM; Janes MS; Pehar M; Monette JS; Ross MF; Hagen TM; Murphy MP; Beckman JS Selective fluorescent imaging of superoxide *in vivo* using ethidium-based probes. Proc. Natl. Acad. Sci. U. S. A 2006, 103, 15038–15043. [PubMed: 17015830]
57. Schieber M; Chandel NS ROS function in redox signaling and oxidative stress. Curr. Biol 2014, 24, R453–R462. [PubMed: 24845678]
58. Sun WH; Liu F; Chen Y; Zhu YC Hydrogen sulfide decreases the levels of ROS by inhibiting mitochondrial complex IV and increasing SOD activities in cardiomyocytes under ischemia/reperfusion. Biochem. Biophys. Res. Commun 2012, 421, 164–169. [PubMed: 22503984]
59. Luo YG; Liu XA; Zheng QS; Wan XM; Ouyang SC; Yin YD; Sui XJ; Liu JJ; Yang XF Hydrogen sulfide prevents hypoxia-induced apoptosis via inhibition of an H_2O_2-activated calcium signaling pathway in mouse hippocampal neurons. Biochem. Biophys. Res. Commun 2012, 425, 473–477. [PubMed: 22846576]
60. Wallace JL Hydrogen sulfide-releasing anti-inflammatory drugs. Trends Pharmacol. Sci 2007, 28, 501–505. [PubMed: 17884186]
61. Han YY; Shang QW; Yao J; Ji Y Hydrogen sulfide: A gaseous signaling molecule modulates tissue homeostasis: implications in ophthalmic diseases. Cell Death Dis 2019, 10, 293. [PubMed: 30926772]
62. Foster JC; Radzinski SC; Zou XL; Finkielstein CV; Matson JB H_2S-releasing polymer micelles for studying selective cell toxicity. Mol. Pharm 2017, 14, 1300–1306. [PubMed: 28300411]
63. Kang JM; Li Z; Organ CL; Park CM; Yang CT; Pacheco A; Wang DF; Lefer DJ; Xian M pH-controlled hydrogen sulfide release for myocardial ischemia-reperfusion injury. J. Am. Chem. Soc 2016, 138, 6336–6339. [PubMed: 27172143]
64. Li L; Whiteman M; Guan YY; Neo KL; Cheng Y; Lee SW; Zhao Y; Baskar R; Tan CH; Moore PK Characterization of a novel, water-soluble hydrogen sulfide - releasing molecule (GYY4137): New insights into the biology of hydrogen sulfide. Circulation 2008, 117, 2351–2360. [PubMed: 18443240]
65. Peng B; Chen W; Liu CR; Rosser EW; Pacheco A; Zhao Y; Aguilar HC; Xian M Fluorescent probes based on nucleophilic substitution-cyclization for hydrogen sulfide detection and bioimaging. Chem.-Eur. J 2014, 20, 1010–1016. [PubMed: 24339269]

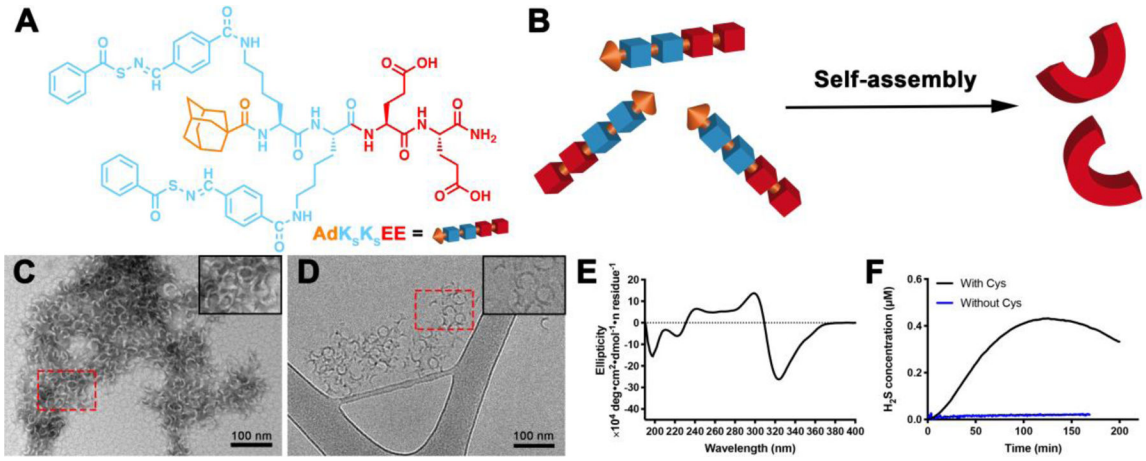

Figure 1.

(A) Molecular structure of PHDC **AdK$_S$K$_S$EE**. (B) Schematic illustration showing self-assembly of **AdK$_S$K$_S$EE** in aqueous solution. (C) Representative conventional TEM micrograph (stained with uranyl acetate, UA), and (D) representative cryo-TEM micrograph of crescent nanostructures formed by PHDC **AdK$_S$K$_S$EE** in phosphate buffer (PB, 10 mM pH 7.4) at 1 mM. Insets in the top right corners of panels C and D show zoomed-in images of the areas outlined by the dashed red rectangles. (E) CD spectrum of **AdK$_S$K$_S$EE** in PB at 100 μM; (F) H_2S release profiles of **AdK$_S$K$_S$EE** triggered by Cys or without Cys in PB at rt. Data were collected on an H_2S-sensitive electrochemical probe from a solution of PHDC (1 mM) and Cys (4 mM) sealed in a well with a gas-permeable membrane inside a vial containing PB (5 mL). Experiments were repeated three times for each PHDC, and data shown reflect averages of the three runs.

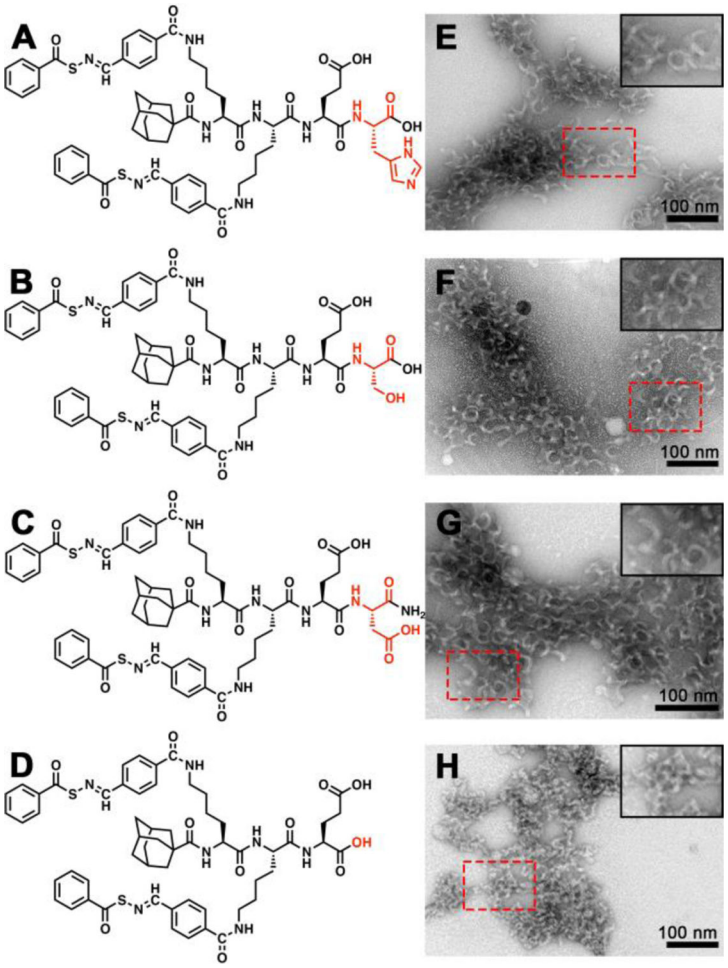

Figure 2.

Molecular structures and conventional TEM images of crescent nanostructures formed by (A, E) **AdK$_S$K$_S$EH**, (B, F) **AdK$_S$K$_S$ES**, (C, G) **AdK$_S$K$_S$ED**, and (D, H) **AdK$_S$K$_S$E** in PB (10 mM pH 7.4). Insets in the top right corners of panels E-H show zoomed-in images of the areas outlined by the dashed red rectangles. Solution concentration: 100 μM. All grids were stained by UA prior to imaging.

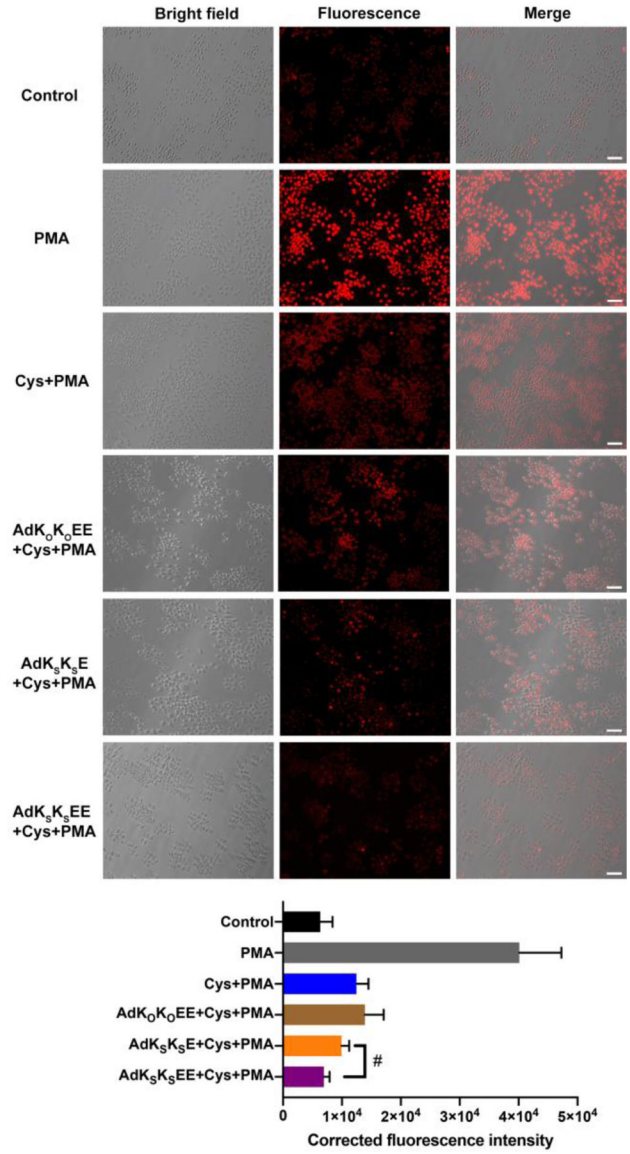

Figure 3.

Bright field, fluorescence, and merged images showing fluorescence in RAW 264.7 macrophage cells pre-incubated with PBS only (row 2, grey bar), Cys (800 μM) (row 3, blue bar), **AdK$_O$K$_O$EE** (200 μM) + Cys (800 μM) (row 4, brown bar), **AdK$_S$K$_S$E** (200 μM) + Cys (800 μM) (row 5, orange bar), or **AdK$_S$K$_S$EE** (200 μM) + Cys (800 μM) (row 6, purple bar) for 30 min before exposure to PMA (1 μg/mL) (groups 2–6) or equal volume of DMSO for 3 h (row 1, black bar). After treatment, cells were incubated with ROS probe DHE (10 μM) for 30 min, washed, and imaged in DPBS by bright-field and fluorescence microscopy. Scale bars are 50 μm. Averaged fluorescence intensities of these six respective treatment groups were quantified by ImageJ (cell counts are > 30 for each group from three separate wells). # indicates $p < 0.05$ for a comparison of the groups indicated as determined by a one-way analysis of variance (ANOVA) with a Student–Newman–Keuls comparisons posthoc test.

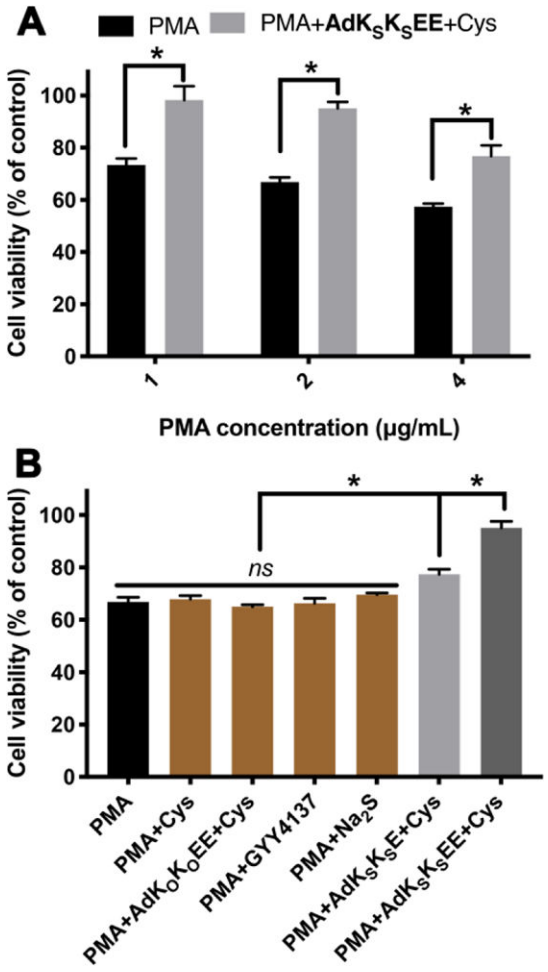

Figure 4.

(A) Cell viability of RAW 264.7 macrophage cells pretreated with **AdK$_S$K$_S$EE** (200 μM) + Cys (800 μM) for 30 min before exposure to different concentrations of PMA for 3 h. * indicates $p < 0.01$ vs PMA. (B) Cell viability of RAW 264.7 macrophage cells pretreated with various controls for 30 min before exposure to PMA (2 μg/mL) for 3 h. Control compound concentrations: Cys, 800 μM; **AdK$_O$K$_O$EE** and **AdK$_S$K$_S$E**, 200 μM; GYY4137 and Na_2S, 400 μM. * indicates $p < 0.01$ among indicated treatment groups. Error bars indicate standard deviation of three separate experiments with five replicates per experiment. Group comparisons are indicated as determined by a one-way analysis of variance (ANOVA) with a Student−Newman−Keuls comparisons posthoc test.

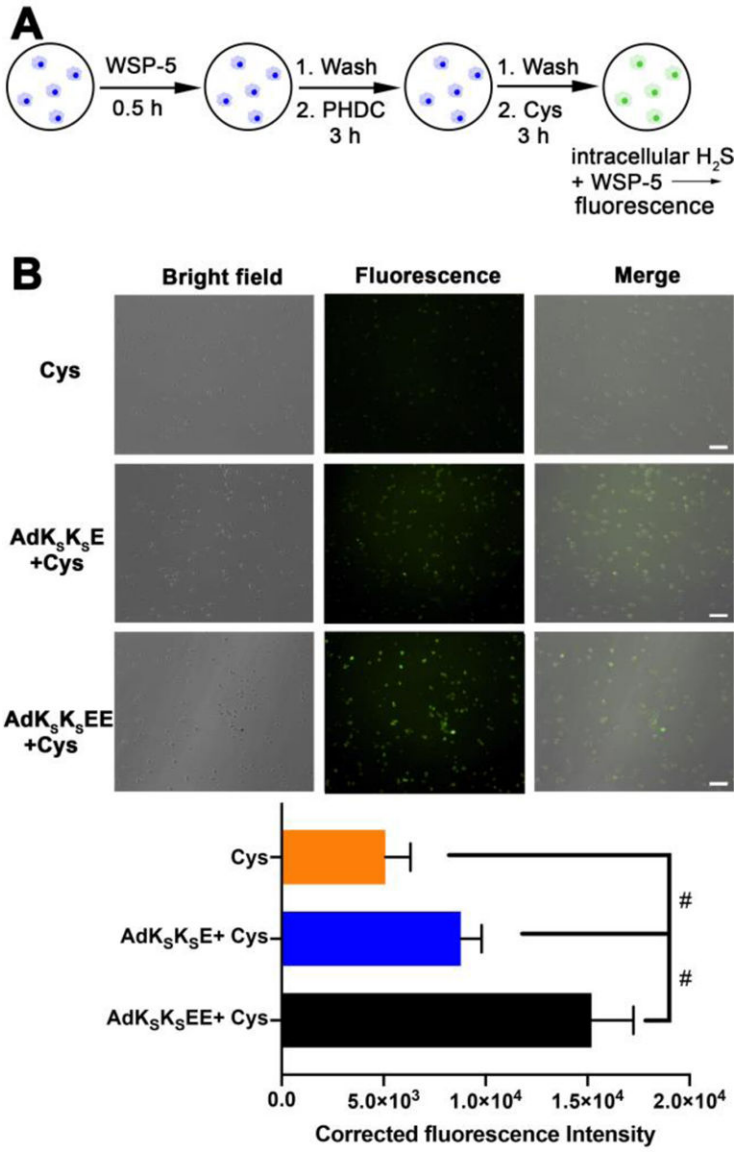

Figure 5.

(A) Illustration showing experimental design for detection of cumulative H_2S release within macrophage cells by WSP-5. (B) Bright field, fluorescence, and merged images showing fluorescence in RAW 264.7 macrophage cells pre-incubated with WSP-5 (50 μM) and CTAB (100 μM) for 30 min, and subsequently treated with PHDCs (**AdK_SK_SE** or **AdK_SK_SEE**, 200 μM) for 3 h, followed by treating with Cys (800 μM) for another 3 h. Cells were then washed, and fluorescence images were taken in DPBS. Scale bars are 50 μm. Averaged fluorescence intensities of these three respective treatment groups were quantified by ImageJ (cell counts are >30 for each group from three separate wells). # indicates $p < 0.05$ for a comparison of the groups indicated as determined by a one-way analysis of variance (ANOVA) with a Student–Newman–Keuls comparisons posthoc test.